OBSERVATION OF FIBRE-FIBRE INTERACTIONS IN SINGLE-FIBRE MODEL SAMPLES

S. Lütze, S. Ritter, G. Busse

Zerstörungsfreie Prüfung, Institut für Kunststoffkunde und Kunststoffprüfung (IKP), Universität Stuttgart, Pfaffenwaldring 32, D-70569 Stuttgart, Germany

SUMMARY: By combining a laser scanning microscope (LSM) with a photoelasticity setup one can investigate the stress field along the fibre-matrix boundary in a polymer composite. Using a special technique, model samples were prepared that contained single glass fibres (d_F=80µm) embedded in a polycarbonate matrix. Tensile stress was applied in situ under the LSM. Phase images of isochromates (lines of equal stress) were calculated from various images taken at the same stress level. We prepared model samples with five equidistant glass fibres that were oriented parallel to the applied load direction. By variation of the distance between the fibres one obtains information on the fibre-fibre and fibre-matrix interaction. Investigations were mainly performed at fibre distances from twice up to five times the fibre diameter.

KEYWORDS: single-fibre model composites, fibre-fibre interaction, in-situ tensile test, fibre break, shear stress behavior, Laser-Scanning Photoelasticity.

INTRODUCTION

The mechanical strength of fibre composites depends on the shear stress between the fibre and the matrix and of the resulting tensile stress in the fibre. That is why single fibre composites (SFC) are being used to investigate the critical fibre length l_C and the maximum of the applicable shear stress [1,2]. Though the SFC-test seems simple the failure of composites is not yet fully understood since there are still numerous statistical and mechanical problems. For an improved understanding one needs to know the stress field around the fibres under load [3]. Besides the SFC-tests exist some more experimental results, e.g. acoustic emission [4] and various microscopy and photoelasticity techniques. Finite Element Modeling and other simulation methods are one way to obtain a better understanding on the micromechanical scale. Using photoelasticity one can well monitor the stress field and how it is affected when fibres in the vicinity are cracking.

SAMPLES AND EXPERIMENTAL SETUP

Sample preparation

As matrix material we used various kinds of polycarbonate (PC3200, PC2000 manufactured by Bayer) where PC3200 has ductile failure while PC2000 fails in a brittle way. Both are technically relevant thermoplastic materials (and not a pure model-material) with a Young's modulus of about 2000 N/mm^2 (see [5] for more details). The statistical data of the glass fibres (diameter d_F = 80μm) that we used have been published by Fiedler [6]. At the length used in our experiments the strength is σ_b=2650 N/mm^2. A special technique had to be developed for embedding fibres parallel to each other at given distances: The fibres are initially long enough so that they hang across a glass plate where they are kept straight by weights at their ends. In this arrangement they are covered by a thin solution of polycarbonate (Fig.1). After evaporation of the thinner they are kept in this position so that they can be cut to the desired length and then be hot pressed between two polycarbonate plates. The data for the pressing process are published by Malter [5]. From the pressed plate material with the embedded fibres a dog-bone tensile test sample is cut where the fibres are oriented along the stress direction.

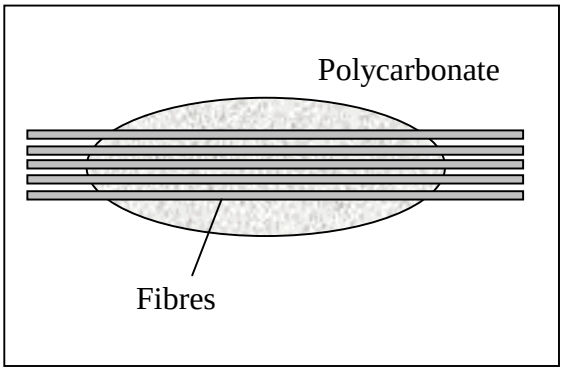

Fig. 1: Preparation of model samples

Photoelastic setup of the laser-scanning microscope and experimental procedure

Unlike standard microscopes the Confocal-Laser-Scanning-Microscopy (LSM) provides information within any particular volume element of a semitransparent specimen. All other information (unfocussed images of planes in other depths) are effectively removed by a spatial filter. This capability has found considerably interest for applications in biology and medicine since it allows to produce three-dimensional images of fluorescent or reflective markers within cells.

A typical arrangement of a scanning optical microscope is shown in [7]. The plane wave emitted by a laser is focussed into a spot on or within the specimen. The light that is locally backscattered from the sample is then focussed by an operationally separate optical system into a spatial filter and therefrom on a detector, thereby discriminating against light from other than the focus plane. This filter (a small pinhole) is located in a plane conjugate to the field. An image of the specimen is generated by scanning the spot across the inspected sample in a rectangular raster pattern (frame rate for 512*512 pixel: 0.5 sec). The lateral and axial resolution depends on the pinhole size, the wavelength of the laser light, and the aperture of the objective. In this confocal arrangement the lateral resolution is slightly better than in the conventional case. The thickness of the optical sections (depth resolution) obtained in the confocal way is ≥ 0.3 μm.

The LS-Microscope that we used in our experiments was a Zeiss LSM 410. It is an invert type microscope with a very stable stand that allows to place the tensile testing machine on the

microscope table and to perform the in-situ tests. The axial shift of the focus is performed by moving the microscope objective.

Photoelasticity

For monochromatic light of wavelength λ, the intensities are described according to the "Wertheim law" [8]

$$I = I_0 \sin^2(\pi N \pm \delta^*) = I_0 \sin^2 \delta^*. \quad (1)$$

Eqn 1 indicates that only the fractional part of the retardation δ* can be determined from the intensity of light while the integer isochromatic order N is lost. By looking at the isochromatic fringe pattern of polariscopes, the maximum evaluable retardation is limited to 0.5 fringe orders. For a more accurate determination of this fractional part a Fourier algorithm is applied to evaluate the phase. On the base of Eqn 1 the intensity I (x, y) is given by

$$I(x, y) = U(x, y)\left(1 + K(x, y)\cos 2(\delta^* + \alpha)\right) \quad (2)$$

where the background intensity U(x, y), the contrast of the fringe pattern intensity K(x, y), and the phase difference δ* are all unknown. The phase α is an added phase difference which is known. Technically this phase shift can be achieved by rotating the analyzer of the polariscope. The phase difference δ* (which characterizes the experimental technique) is the parameter of interest. Thus, a minimum of three equations is needed to solve for δ*. Values of α between 0 and 2π are chosen to provide the necessary equations to solve for α. Various algorithms have been used. As the intensity changes twice between 0 and 2π, a three-shift method is applied to provide intensities I_1 to I_3 at any point corresponding to the added phase differences of $\alpha_1 = 0$, $\alpha_2 = 1/3\pi$ and $\alpha_3 = -1/3\pi$ (Fig. 2). The phase difference δ* is then calculated according

$$\delta^* = \arctan\left(\sqrt{3}\,\frac{I_3 - I_1}{2I_2 - I_3 - I_1}\right). \quad (3)$$

Also the determination of the absolute fringe order N becomes easier, because the increase or decrease of the absolute fringe order can be evaluated.

Laser-Scanning-Photoelasticity

The polarisation setup combined with the LSM has been described previously [7]. By focussing on the boundary-surface of the matrix and the surrounding air the reflected light is detected. In terms of photoelasticity this is a circular-reflection-polariscope. The effective optical thickness d´ is twice the geometrical thickness d of the test specimen. The resulting equation to calculate the phase lag is then

$$\Delta = 2C_0 d \cdot (\sigma_1 - \sigma_2). \quad (4)$$

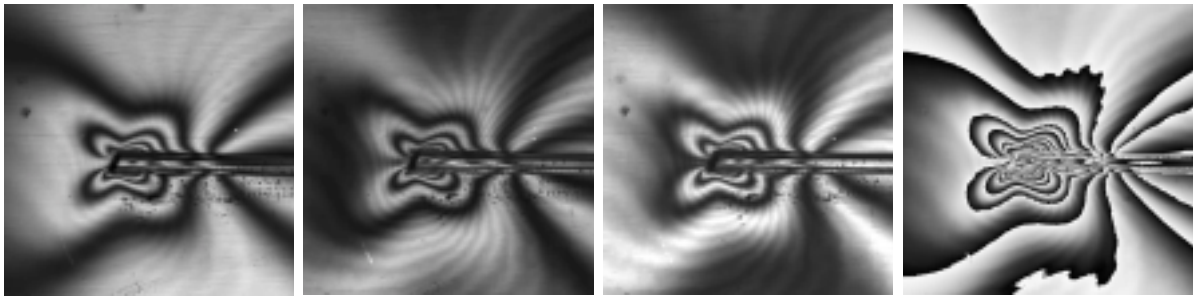

$\alpha_1 = 0$ $\alpha_2 = 1/3\pi$ $\alpha_3 = 1/3\pi$ phase-image

Fig. 2: Three isochromatic fringe patterns are taken with different phase shifts α. The phase image is calculated according to Eqn 4.

The samples described above are loaded by the tensile testing machine at levels that increase in steps of $\Delta\sigma_S$=2N/mm². At each load level three images I_1, I_2 and I_3 are taken each with a different analyser angle (see Eqn 3) in order to determine therefrom the phase image. After calibration of the photoelasticity data on samples without fibres it is possible to obtain quantitative data on the single fibres samples. The stress field is evaluated along the fibres [5,7].

EXPERIMENTAL RESULTS

Comparison of samples with equal fibre-fibre distances.

To make the results more reliable we performed measurements on several samples. Though they had been prepared in the same way, cracking of the fibres occurred at different levels of load which is due to the statistical distribution of the fibres [6]. The stress distribution for three samples with a fibre-fibre distance $d_A=4d_F$ is shown in Fig. 3 for the load level 34 N/mm^2. Evaluation was performed along the central fibre. The stress maximum at the ends is about the same in the three curves, in our experiments it never differed by more than 5 N/mm^2. Fig. 4 was obtained at three different levels of load where sample 22 cracked while sample 23 did not. In order to analyse the consequence of the fibre crack on the next and overnext fibre, these fibres were evaluated at two of the indicated three load levels, as shown in Fig. 5 and 6. Comparison of the images shows how the crack induces a stress enhancement for the central fibre (the vertical isochromate lines are tilted due to the crack). All data sets were normalized to the same length in order to eliminate this influence. The results are given in Fig. 5 and Fig. 6 for the overnext and the next fibre, respectively.

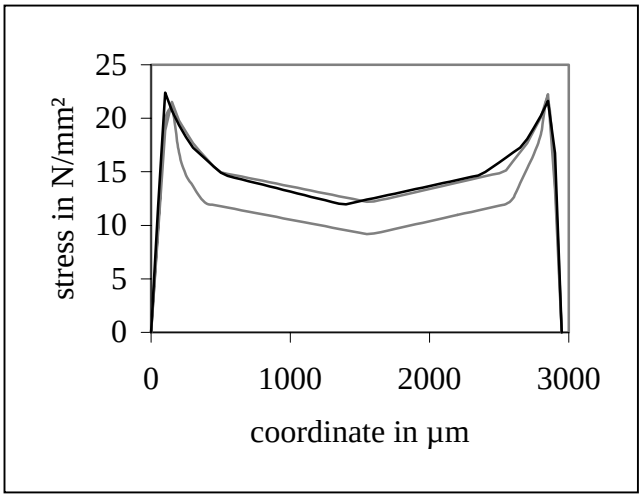

Fig. 3: Stress along the central fibre for several samples having the same fibre-fibre-distance. Load is 34 N/mm^2 for all samples.

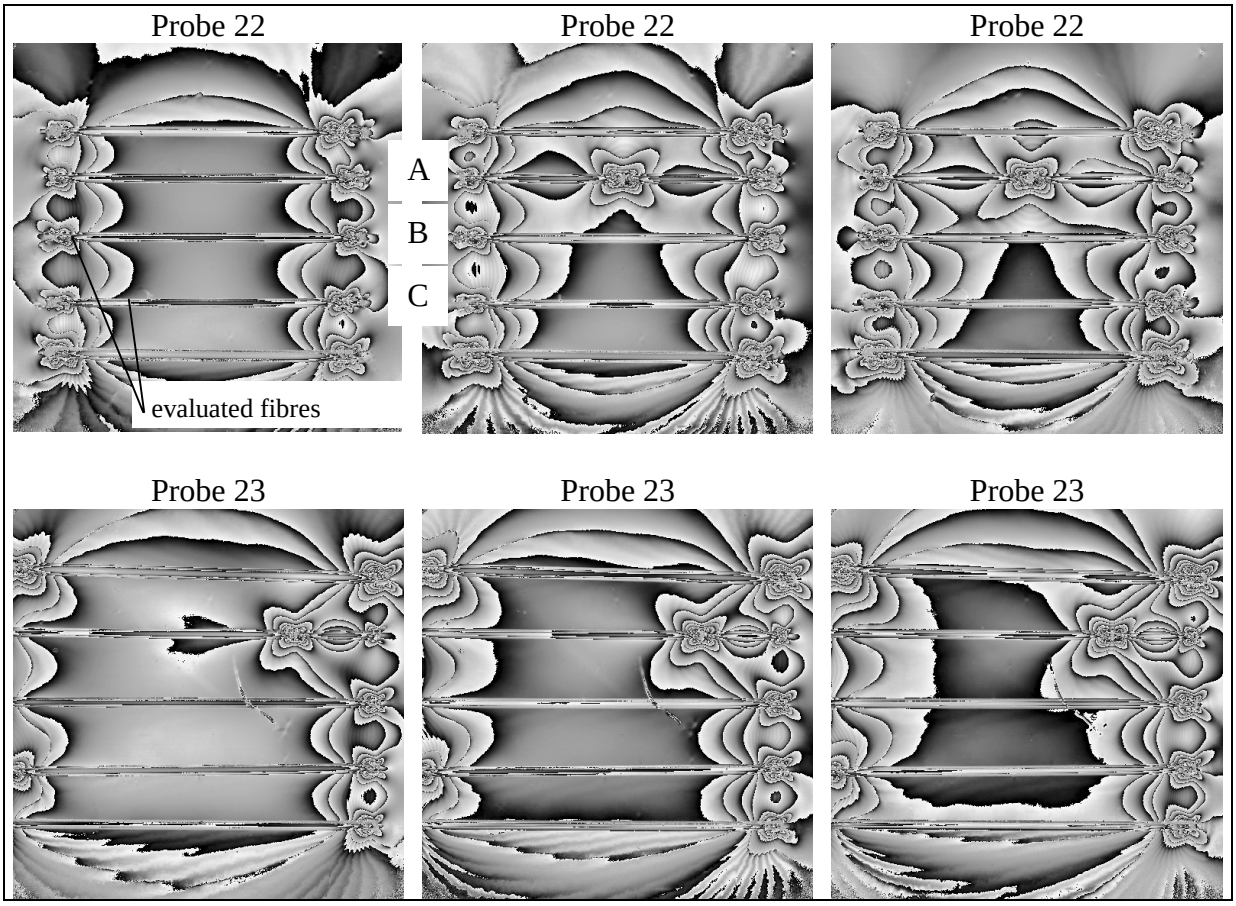

Fig. 4: Phase images of isochromates. Top: Crack near center of fibre A and its influence on fibres B and C. Bottom: Crack close to fibre end (not much influence on stess field). External stress level increases from 44N/mm^2 (left) via 48N/mm^2 (middle) to 54N/mm^2 (right).

Fig. 5 indicates how the stress profile along fibre C changes when the increase of load causes a crack in fibre A which is the overnext neighbour. The shape remains essentially the same except for the height which has increased due to the extra load step. However, for the next neighbour (fibre B) a change of shape is clearly visible (Fig. 6). The length of the central plateau (indicated by short vertical lines) decreases and the distance between the peaks becomes smaller. So at this fibre-fibre distance the overnext neighbour is obviously well shielded against the effect of fibre crack.

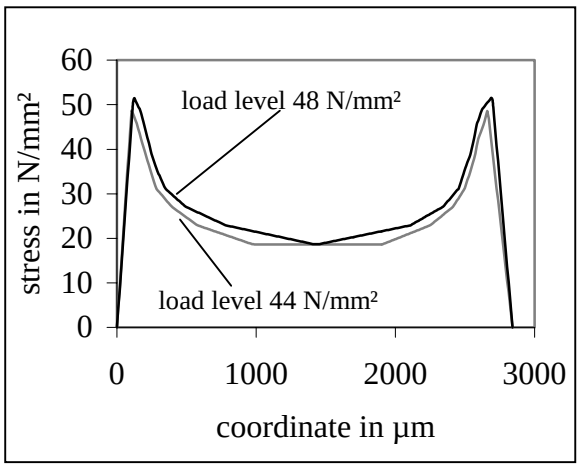

Fig. 5: Effect of crack in fibre A on overnext fibre C.

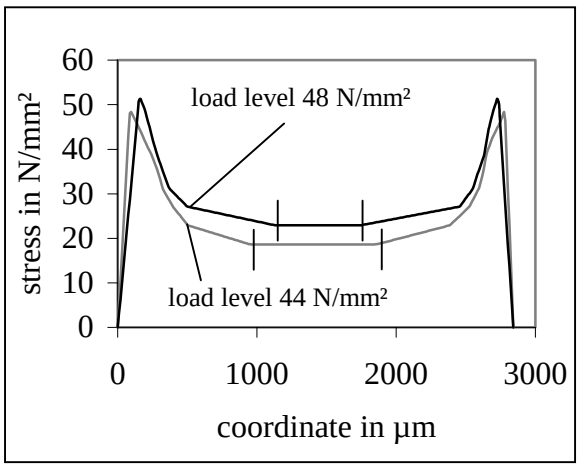

Fig. 6: Stress along fibre B before and after crack of neighbour fibre A.

Comparison of samples with different fibre-fibre-distances

Fig. 7 shows how the stress along the central fibre changes when the distance between the fibres is modified in four steps from $2d_F$ to $5d_F$ while the external stress is at a level where no crack occurred (44 N/mm^2). The distance range between $0d_F$ and $1d_F$ could not be investigated due to the resolution of the microscope. The stress distribution is not sensitive to the distance if it is below $4d_F$, so there is a saturation of the shielding effect provided by the neighbouring fibres. Stress at the ends of the fibre increases if the distance to the next fibre is $5d_F$, so the shielding effect becomes weaker. Fig. 8 and Fig. 9 show how fibre distance affects the influence of a cracking fibre on its next neighbour (indicated by arrow). Topics of interest are the range of this influence and the increase of stress on the neighbour depending on its distance. The external stress was 52 N/mm^2, distances were between $1.7d_F$ and $3.8d_F$. The influence of a fibre crack on the neighbour fibre increases with decreasing distance. Additionally the stress along the center of the fibre is no longer constant, it rather displays local fluctuations (see Fig. 10).

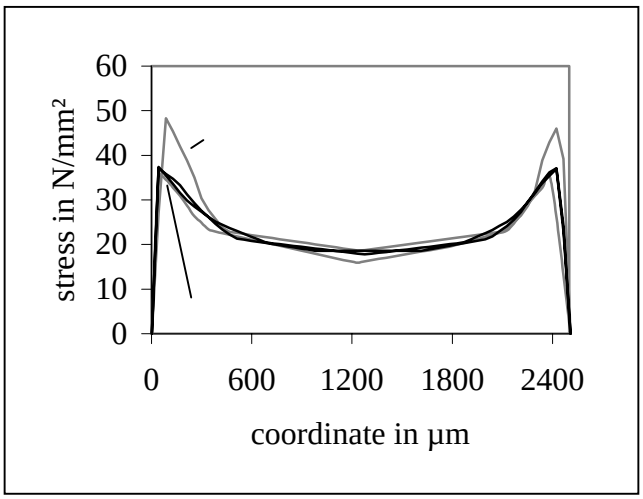

Fig. 7: Stress along fibre for various fibre-fibre-distances.

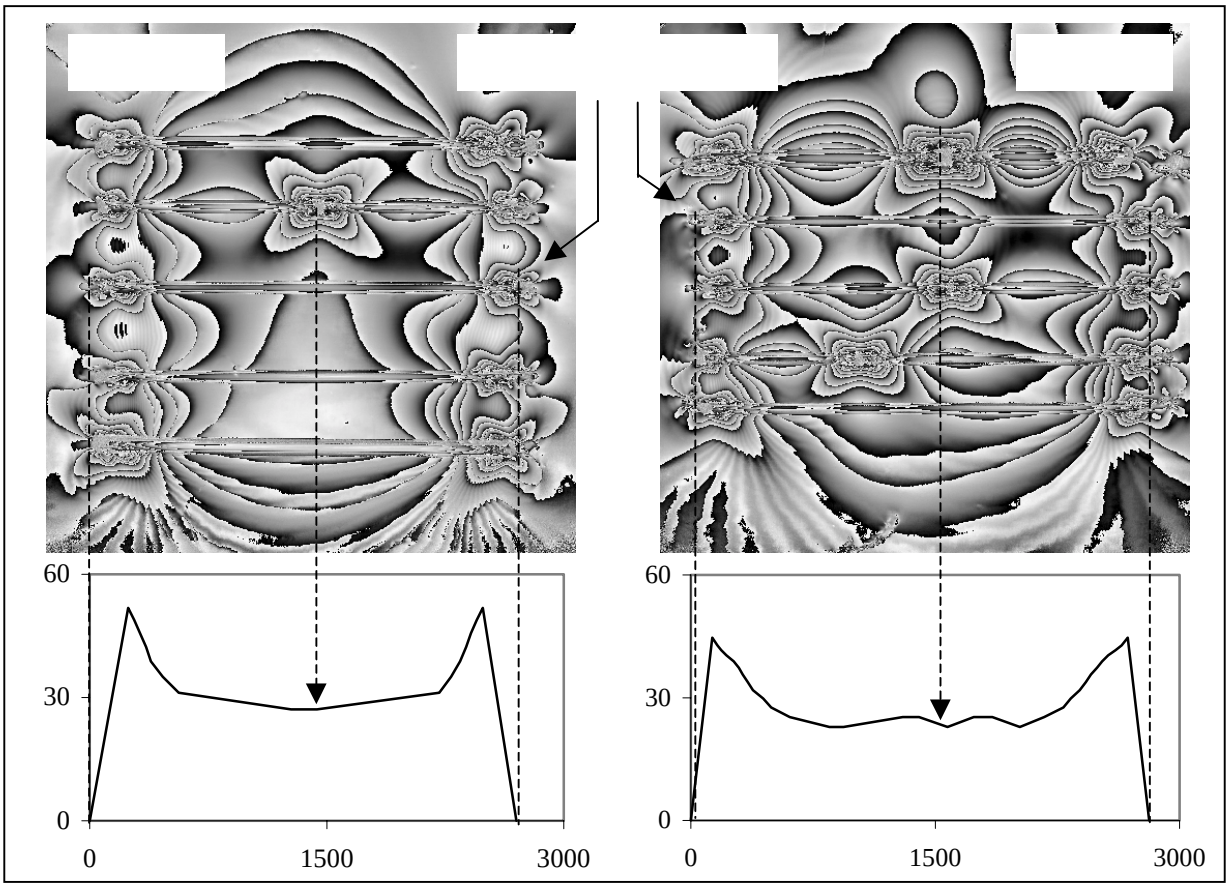

Fig. 8: Phase images of isochromates and stress along fibre as calculated therefrom. (part 1)

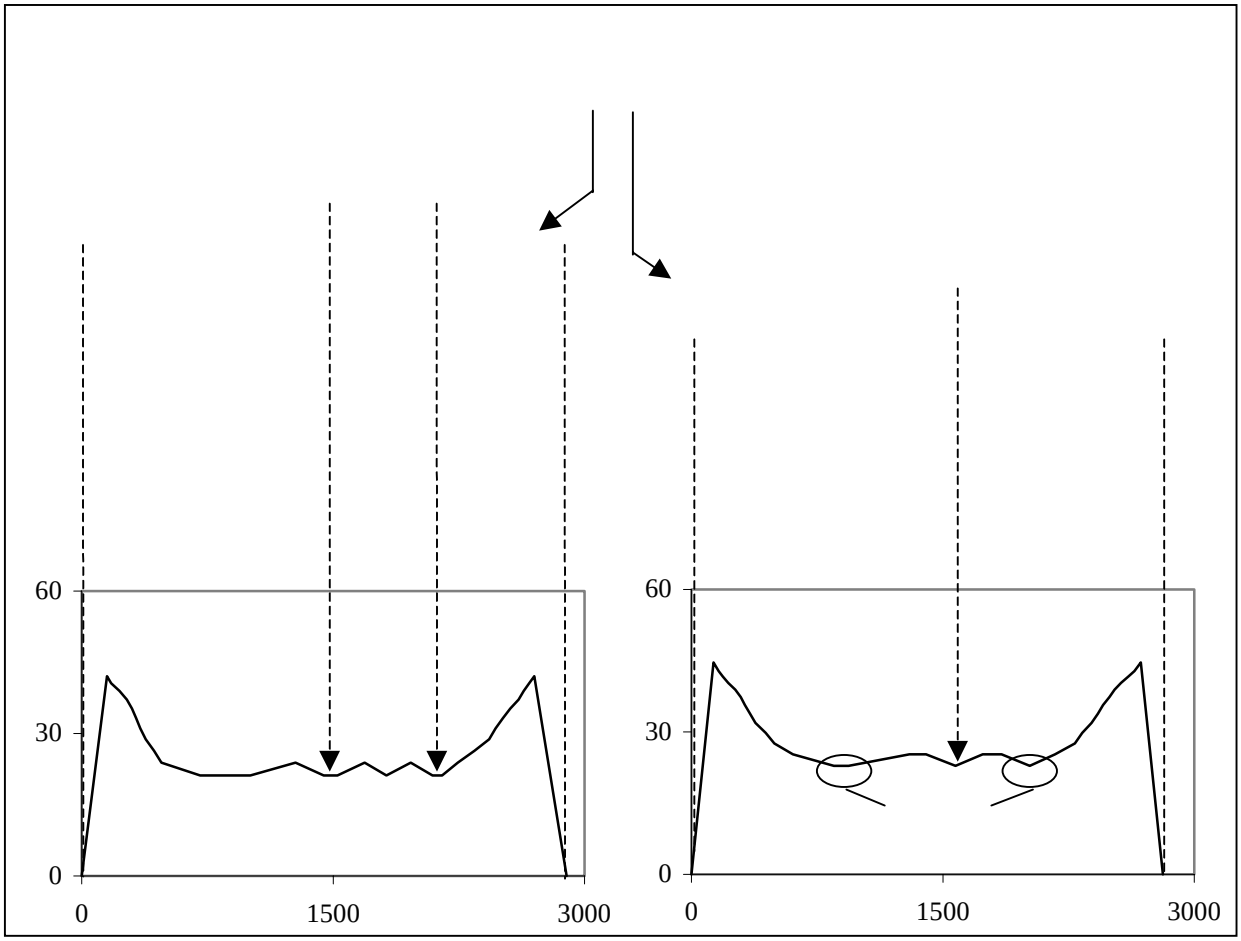

Fig. 9: Phase images of isochromates and stress along fibre as calculated therefrom. (part 2)

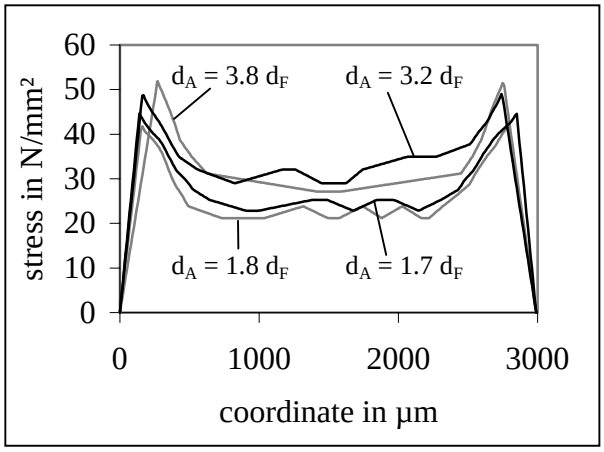

Fig. 10: Stress along fibre after crack at next fibre (for various fibre-fibre-distances).

In our experiments we found that cracks will likely occur in minima as those indicated as "predicted cracks" in Fig. 9. As this stress modulation becomes stronger at smaller distances (see Fig. 10), the location of the next fibre crack can be predicted with a higher probability if the cracking fibre is closer. Also it should be mentioned that the minimum close to the location of the crack is not as strong as the adjacent minima (Fig. 9, minimum between predicted next cracks), and in disagreement to [6] cracks were rare in this location. However, we do not yet have enough statistical material on this effect since the main interest of our investigations was the shielding effect in fibre arrays.

CONCLUSIONS

We investigated arrays of 5 parallel fibres in a polycarbonate matrix in order to see how the stress fields interact with each other, also after cracking. We found a shielding effect and also a local stress modulation induced by a crack on the neighbouring fibres, if they are close enough. Though some results are not unexpected qualitatively, they are not fully understood on a quantitative base. Therefore presently a numerical simulation is performed for the stress fields along the fibres in order to see e.g. how the increase of stress is related to fibre distances and how well these theoretical results compare to the experimental results.

ACKNOWLEDGMENTS

This work has been supported financially by the Deutsche Forschungsgemeinschaft (DFG / SFB 381, project B1). The authors are grateful to A. Burkert / Carl Zeiss and the Carl Zeiss Jena GmbH for good cooperation. The authors would like to thank U. Malter for the skillful preparation and testing of the samples.

REFERENCES

1. A. Kelly, W. R. Tyson, "Tensile properties of fibre-reinforced metals: Copper/Tungsten and Copper/Molybdenum", Mech. Phys. Solids, Vol.13, 1965, pp. 329-350.

2. L. Dilandro, A. T. Dibenedetto and J. Groeger, "The effect of fiber-matrix stress transfer on the strength of fiber-reinforced composite materials", Polymer Composites, Vol. 9, No. 3, 1988, pp. 209-221.

3. M. R. Nedele and M. R. Wisnom, "Finite element micromechanical modelling of a unidirectional composite subjected to axial shear loading", Composites, Vol. 25, 1994, pp. 263-272.

4. T. Bidlingmaier, A. Wanner, S. Ritter, "Quantitative Analyse der Schallemission von Schädingungsprozessen in Faserverbundwerkstoffen mit duktiler Matrix", DGZfP Berichtsband, Vol. 58, 1997, pp. 47.

5. U. Malter, "Einzelfaserverstärkte Polycarbonat-Zugproben: Die Herstellung sowie die experimentelle Darstellung unterschiedlicher Schädigungsmechanismen", Studienarbeit Institut für Kunststoffprüfung und Kunststoffkunde, 1997.

6. B. Fiedler, "Micromechanische Betrachtung der Lasteinleitung und Lastübertragung in Faserverstärkten Polymeren", Dissertation Universität Hamburg Harburg, 1998.

7. S. Ritter, “In-Situ Observation of the stress field of the failure Process in single fibre reinforced polymers”, Quantitative nondestructive evaluation, Vol. 17B, 1998, pp. 1201-1208.

8. H. Wolf, "Spannungsoptik Band 1", Springer Verlag Berlin, 1976.

9. P. W. J. Heuvel van den, Y. J. W. Bruggen van der and T. Peijs, "Failure phenomena in multi-fibre model composites. Part 1: An experimental investigation into the influence of fibre spacing and fibre/matrix adhesion", Composites Part A, Vol. 27A, 1996, pp.855-859.